Geometric shapes effect of in-duct perforated orifices on aeroacoustics damping performances at low Helmholtz and Strouhal number

Zhao, Dan; Ji, Chenzhen; Wang, Bing

2019

https://hdl.handle.net/10356/85244

https://doi.org/10.1121/1.5096642

Geometric shapes effect of in-duct perforated orifices on aeroacoustics damping performances at low Helmholtz and Strouhal number

Dan Zhao[a)]
Department of Mechanical Engineering, University of Canterbury, Christchurch, 8140, New Zealand

Chenzhen Ji
College of Engineering, Nanyang Technological University, Singapore 639798, Singapore

Bing Wang
School of Aerospace Engineering, Tsinghua University, Beijing, 100084, China

In this work, experimental studies are conducted to measure the aeroacoustics damping performances of 11 in-duct perforated plates in a cold-flow pipe with a variable Mach number. These in-duct plates have the same porosities but different number N and geometric shaped orifices. Here six shapes are considered, i.e., (1) triangle, (2) square, (3) pentagon, (4) hexagon, (5) star, and (6) circle. It is shown that the orifice shape has little influence on power absorption Δ and reflection coefficient R at a lower Helmholtz number He ≤ 0.0903. However, as He is increased, the in-duct plate with a star-shaped orifice is shown to be with much lower Δ in comparison with that of other plates with different shape orifices. In addition, the perforated orifice with the same shape and porosity but a larger N is shown to be associated with 20% more power absorption at approximately He $= 0.1244$. Δ_{max} is observed to be approximately 85% at about He $= 0.0244$, as $M_a \approx 0.029$. To gain more insights, the quasi-steady model is applied, depending on the Strouhal number Sr. The transition from quasi-steady flow behaviors to unsteady behaviors occurs at approximately Sr $= 0.45$. The measured minimum reflection coefficient R_{min} occurs at $M_a \approx 0.024$. This experimental finding is consistent with the quasi-steady prediction.

[DES]
Pages: 2126–2137

NOMENCLATURE

A_o	total area of the perforated orifices, m²
A_p	cross-sectional area of the pipe, m²
[A]	4×4 coefficient matrix involved in Eq. (7) and the Appendix
c_s	sound speed, m/s
$\hat{C}, \hat{Q}$	the real and imaginary part of $\hat{S}$
D_d	inner diameter of the pipe, 44 mm
f	forcing frequency $f = \omega/2\pi$, Hz
He	Helmholtz number
$\hat{H}_{mn}$	transfer function between sensor m and n
k_i, k_r	wave number
L_d	downstream pipe length, 0.8 m
M_a	Mach number of the mean pipe flow
N	the number of perforated orifices
$\tilde{p}_{i,r}$	incident and reflected acoustic fluctuations, Pa
R	reflection coefficient
Re, Im	real and imaginary part of a given complex variable
$\hat{S}_{AA}, \hat{S}_{BB}$	auto-spectral density of the incident and reflected sound waves upstream
$\hat{S}_{CC}, \hat{S}_{DD}$	auto-spectral density of the incident and reflected sound waves downstream
$\hat{S}_{12}, \hat{S}_{11}$	cross- or auto-spectral density of the measurement from sensor 1 and/or 2
Sr	the Strouhal number
St_o	the Stokes number
T_w	thickness of the perforated plate, 2 mm
T_p	the period of data logging
V, v	the mean and fluctuating flow velocity in the pipe, m/s
x	the axial coordinate, m
η	porosity
ω	forcing frequency, rad/s
$\hat{\Phi}$	phase difference between sensors 1 and 2
Δ	power absorption coefficient
$*$	complex conjugate

I. INTRODUCTION

To dampen unwanted noise or to mitigate thermo-acoustic instabilities,[1] perforated liners are widely used as acoustic dampers.[2] They are usually metal sheets consisting of thousands of tiny perforated orifices.[3] In some practical applications, for example, in gas turbines or aero-engines,[4] a cooling air flow is needed to pass through the orifices to prevent the liners from being burned or damaged due to the combusting flow. The mean flow through the perforated plates is also known as bias flow.[1] The main noise damping

a)Electronic mail: dan.zhao@canterbury.ac.nz

mechanism of such liner involves thermoviscous effect and/ or vortex shedding produced over the rims/edges of the tiny orifices. When working fluids are flowing through the orifices, an unsteady "jet" is produced. It then undergoes viscous dissipation to convert acoustic perturbations into nonradiating vortical perturbations.

Over the past few decades, intensive and extensive research[4–8] is conducted to perforated liners, aiming to better understand its damping mechanism and optimize its performance. Both numerical,[4,5] theoretical,[6] and experimental investigations[7,8] are conducted. Most of the experimental studies are concerned with measuring the power absorption, transmission loss coefficient, or acoustic impedance of perforated liners. This is most likely because the parameters are easier to be experimentally determined in comparison with the vorticity-involved flow field near the perforated orifices,[9] which are typically with a diameter of 1–2 mm. Hughes and Dowling[10] conducted an experimental measurement on a perforated plate with a backed screen. It was shown that almost 100% incident sound on a perforated liner might be dissipated in the presence of a bias (cooling) flow. Jing and Sun[8] conducted a similar experimental measurement on a perforated plate in the presence of a bias flow. They found that not only the bias flow Mach number but also the orifice thickness play critical roles on affecting the power absorption and acoustic impedance characterizing the liner's damping performance. Later, Eldredge and Dowling[11] confirmed Jing and Sun's[8] finding by measuring the noise damping effect of a double-layer perforated liner attached to a cold-flow pipe in the presence of both grazing and bias flows. They found that the maximum power absorption coefficient could be 80%, depending on the axial location of the liner and the bias flow Mach number. Grace et al.[12] theoretically showed that the shape of the orifice affects the Rayleigh conductivity. However, no experimental studies are conducted. Lack of this investigation on the effect of perforated orifice shape partially motivated the present work.

Besides experimental studies, numerical investigations of the damping mechanism and performance of perforated orifices are intensively conducted either in time- or frequency- domain.[6,11,13,14] Howe[13] used Rayleigh conductivity to capture the noise damping effect of a single orifice via the periodic shedding of vorticity at a high Reynolds-number. Howe's model was extended by Wendoloski[6] by using Green's function to study the damping performance of a perforated orifice in a flow duct. It was found that there is an optimum porosity (open area ratio) of approximately 0.3 corresponding to the maximum damping performance. The Rayleigh conductivity model is modified to simulate the dissipation of axial plane waves using a double-layer perforated liner in the presence of a bias flow.[11] Kierkegaard et al.[14] modelled the wave propagation in a flow duct by linearizing Navier-Stokes (NS) equations in frequency domain.

Compared with numerical modeling in frequency domain,[11,15] time-domain numerical simulations[16–19] can provide useful information such as transient flow and sound propagation, which is not available in frequency-domain studies. Two-dimensional (2D) direct numerical simulation (DNS) was performed by Tam et al.[17] to gain insight on the damping mechanism and performance of a single aperture. It was found that

vortex shedding was the dominant damping mechanism, as incident sound intensity is high. Three-dimensional (3D) DNS simulations[19] were conducted to predict the acoustics absorption behavior of a honeycomb liner. The orifice boundary layer was shown to play an important role in affecting the nonlinearity. 2D compressible large-eddy simulations (LES) were conducted by Mendez and Eldredge[18] to study time evolution of the flow-sound interaction through single or multiple perforated orifices.

Recently, Su et al.[20] conducted 2D unsteady Reynolds averaged NS simulation via OpenFOAM to study the acoustic behavior of an orifice. They claimed that the computational fluid dynamics (CFD) approach can correctly predict the acoustic response of a turbulent flow through an orifice. The conventional unsteady Reynolds-averaged Navier-Stokes (URANS), LES, or DNS simulations as described above involve using finite difference or finite volume methods to solve the NS equations.[21] As a promising but alternative numerical tool, lattice Boltzmann (LBM) simulations[5,22–25] could also be conducted to study the noise damping mechanism of perforated orifices/plates. Ji and Zhao[5,22] conducted a 3D LBM simulation to study the noise damping performance of a circular orifice, as a bias flow is present. Comparison is then made between the vortex sheddings from the square and circular shaped orifice as shown in Fig. 1.

The flow conditions and the porosity are all the same. Further study on the edge shape effect was performed by conducting 2D LBM simulations.[22] Foregoing studies are concerned with the mean flow or porosity effect of in-duct square- or circle-shaped orifices. However, perforated plates with the same porosity but different number and shaped orifices have not been experimentally examined. This partially motivated the present study.
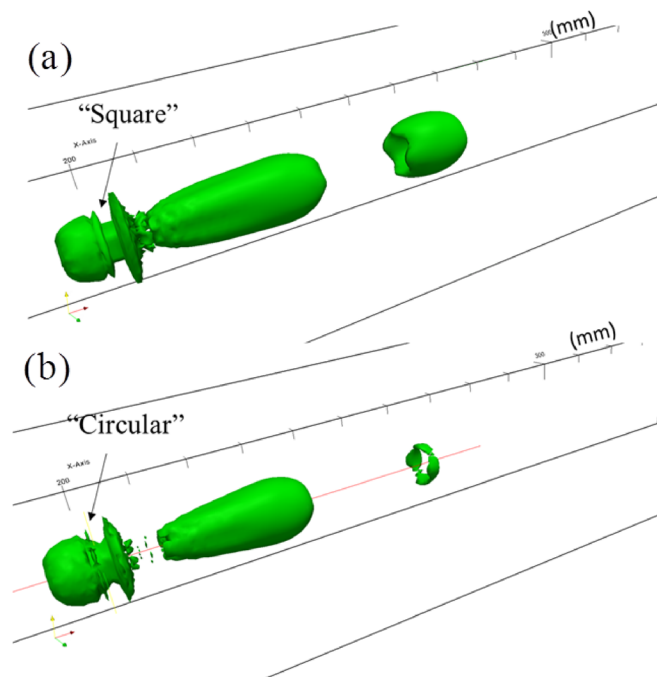

FIG. 1. (Color online) Vortex shedding produced from a (a) square (Sq) and (b) circle (Ci) orifice, when the incident sound wave is set to $\omega/2\pi = 382$ Hz. (a) and (b) Iso-surfaces of vorticity magnitude at constant value of 15.8. The numerical simulations are done by applying a periodic flow fluctuation of 10 Pa at upstream, when there is no mean flow.

In this work, experimental studies are conducted to determine the acoustic damping performance of a series of in-duct perforated orifices in the presence of a low Mach bias flow. Emphasis is being placed on the effects of (1) the geometric shape, (2) the number N of orifices, and (3) the mean bias flow Mach number M_a. The experimental setup is described in Sec. II. Eleven in-duct orifices with the same porosity of 4% but different geometric shapes of (1) triangle (Tr), (2) square (Sq), (3) pentagon (Pe), (4) hexagon (Hx), (5) star (St), and (6) circle (Ci) are manufactured. To characterize and quantify the orifices' acoustic damping effects, power absorption coefficient Δ and reflection coefficient R are defined and measured. This is described in Sec. III. The classical two-microphone method is reviewed and applied to decompose the plane waves propagating in the cold-flow pipe. In addition, three non-dimensional parameters such as Helmholtz, Stokes, and Strouhal numbers are introduced. This enables the present experimental studies to be more generalized. In Sec. IV, these in-duct orifice damping performances are discussed, as the geometric shape, the number of orifices, or the mean bias flow Mach number is varied. Comparison is then made to obtain the optimum design. In Sec. V, a quasi-steady study of perforated orifices is conducted to shed light on the optimum Mach number (corresponding to the minimum reflection coefficient R_{min}) Finally, in Sec. VI, key findings are summarized.

II. DESCRIPTION OF EXPERIMENTAL SETUP

To study its aeroacoustics damping performance,[26–29] a cold-flow axial duct system in the presence of an in-duct perforated plate is designed and tested. The schematic of the experimental pipe system with the perforated plate implemented is shown in Fig. 2. To simulate practical applications, there is a mean flow forcing to pass through the perforated plate. The imposed mean flow is used for cooling purposes and it is also known as bias flow. The mean flow is produced and controlled by a centrifugal pump. To achieve uniform and steady bias flow, a large diffusing cavity/box is applied and connected to the inlet of the lined duct. The mean flow speed through the duct is measured by using a hot wire anemometer (Dantec-MiniCTA-54T42; Dantec, Skovlunde, Denmark) in the large cavity inlet. The maximum flow rate through the duct is approximately 0.02 m³/s. A loudspeaker driven by a digital function generator and an amplifier is enclosed inside the diffusing box to produce axial plane waves. The loudspeaker is Alda Series X (8 Ohm) and its maximum output power is 100 W. The sound pressure level is between 90 and 120 dB. The forcing frequency is between 100 and 1000 Hz, which is well below the cut-on frequency of the first radial mode of approximately 3300 Hz. The measured frequency range is chosen so that the loudspeaker and the microphones are associated with a "flat" response. In addition, the axial distance between the neighboring microphones are fixed during the experimental tests. Higher frequency measurements could be done by calibrating the microphones and reducing the axial distance of these microphones. The produced sound waves are superimposed with the mean cooling flow. These waves propagate through the in-duct perforated orifices and are blown out of the pipe.

To record the acoustic pressure perturbations, two arrays of B&K 4957 microphones (Brüel & Kjær, Nærum, Denmark) are implemented. One array is placed on the upstream of the pipe with an axial distance of 10 cm. The other array is flush mounted downstream with an axial distance of 10 cm. The cylindrical duct to each side of the perforated plate is open. The length and inner diameter of the downstream of the pipe is $L_d = 0.8$ m and $D_d = 44$ mm, respectively. There are 11 in-duct perforated plates with the same thickness of $T_w = 2$ mm and the same porosity of 4% being fabricated. The orifices of each perforated plate have different number N and geometric shapes such as (1) triangle, (2) square, (3) pentagon, (4) hexagon, (5) star, and (6) circle as shown in Fig. 3. The circle-shaped orifice is widely
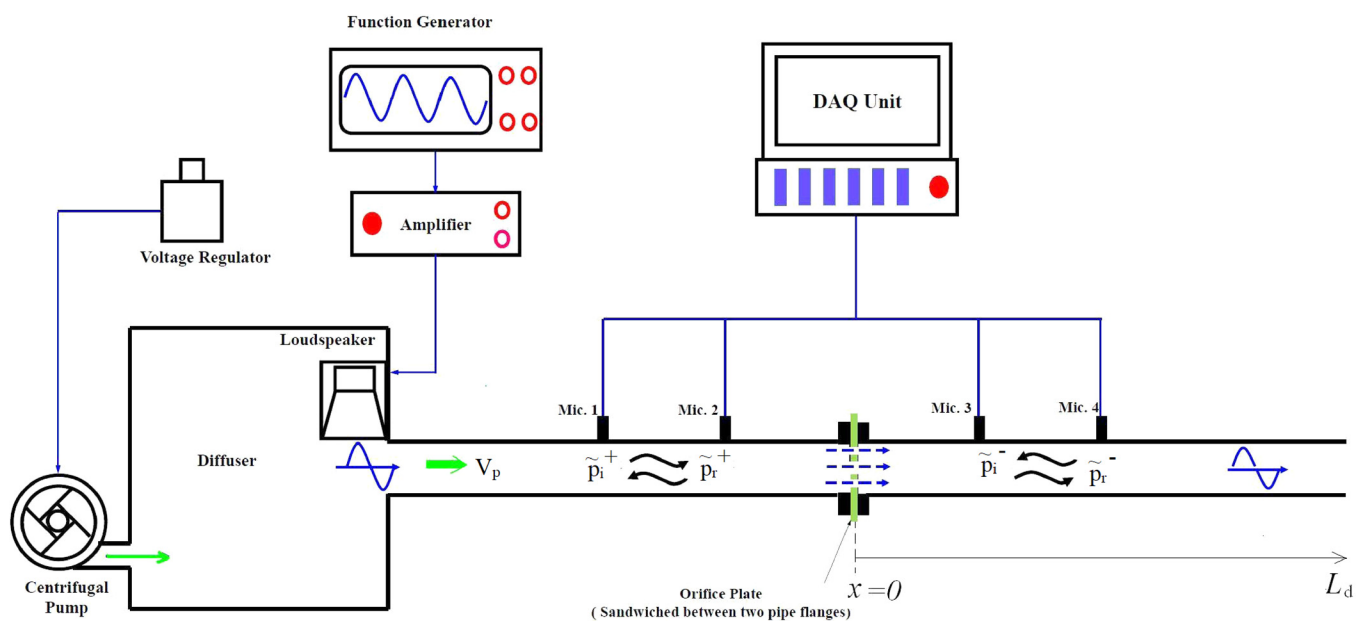

FIG. 2. (Color online) Schematic of experimental setup with a mean flow present and an in-duct orifice plate implemented.
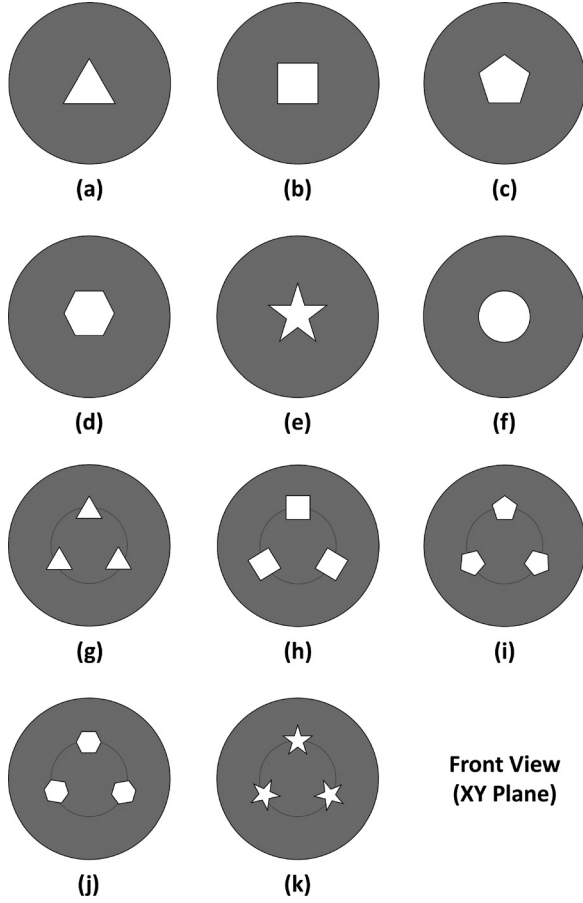
FIG. 3. Front view of different geometric shapes of the 11 perforated plates.

III. CHARACTERIZING AEROACOUSTICS DAMPING PERFORMANCE AND DEFINITION OF DIMENSIONLESS PARAMETERS

The microphones are calibrated to minimize measurement errors. Here the calibration is done by using a piston phone [sound pressure level (SPL) of 94 dB at 1 kHz] and a calibration box. All microphones in the calibration box as shown in Fig. 4(a) are expected to measure the same pressure amplitude with zero phase difference in theory. However, the measured gains and phases shift might be somehow different due to the sensor manufacturing. Such a difference needs to be considered in measuring the power absorption Δ and reflection coefficient R of the in-duct perforated orifices.

Following the previous works,[30,31] microphone calibration is achieved by determining a transfer function in frequency domain, as these microphones are excited by the same sound waves. The transfer function $\hat{H}_{12}(\omega)$ between sensors/microphones 1 and 2 is estimated as

$$\hat{H}_{12}(\omega) = \hat{S}_{12}(\omega)/\hat{S}_{11}(\omega), \tag{1}$$

where $\hat{S}_{12}(\omega)$ is the cross-spectral density between the experimental measurements from pressure sensors 1 and 2, ω is the noise frequency, $\hat{S}_{11}(\omega)$ is the auto-spectral density of the measurement from the pressure sensor 1, and $|\hat{H}_{12}(\omega)|$ is the gain between pressure sensors 1 and 2. The phases shift/difference between pressure sensors 1 and 2 is characterized by $\hat{\Phi}_{12}(\omega)$. It can be determined by

$$\hat{\Phi}_{12}(\omega) = \tan^{-1}\left\{\frac{\mathrm{Im}\left[\hat{H}_{12}(\omega)\right]}{\mathrm{Re}\left[\hat{H}_{12}(\omega)\right]}\right\}, \tag{2}$$

where $\mathrm{Re}\{\cdot\}$ and $\mathrm{Im}\{\cdot\}$ denote the real and imaginary parts of $\hat{H}_{12}(\omega)$, respectively.

The loudspeaker placed in the calibration box is driven by the digital function generator. It produces a sinusoid signal between 100 and 1000 Hz. The frequency is varied with a step of 10 Hz. It is found that the SPL of the produced noise is between 90 and 130 dB, as measured by a sound level meter. LabVIEW2010 is applied for data logging. The acoustic pressure perturbation is recorded at a sampling rate of 10 000 Hz. The measured acoustic fluctuations from these

used in practice, as shown in Fig. 3(f). The geometry, dimensions of these orifices, and the mean flow conditions are summarized in Table I. For comparison, the number of perforated orifices is varied for the perforated plates with the same porosity and same shaped orifices. For example, perforated plates (a) and (g) are associated with triangle-shaped (Tr) orifices. Their porosities are the same as $\eta = 4\%$. However, the number N of the orifices is increased from 1 to 3. The duct cross-sectional area A_p is approximately 1963.5 mm^2. The porosity η is determined by $\eta = A_o/A_p$. Here A_o is the total area of the perforated orifices.

TABLE I. Geometry and flow conditions of the perforated plates with different shapes and dimensions of tiny orifices. A_0 is the total open area of the orifices.

Perforated Plate	Orifice dimensions				Orifice Shape	Bias Flow Mach Number M_a
	A_0(mm^2)	T_w(mm)	Porosity η	Number of orifices N		
a	78.54	2	4%	1	Triangle	$0 \rightarrow 0.036$
b	78.54	2	4%	1	Square	$0 \rightarrow 0.036$
c	78.54	2	4%	1	Pentagon	$0 \rightarrow 0.036$
d	78.54	2	4%	1	Hexagon	$0 \rightarrow 0.036$
e	78.54	2	4%	1	Star	$0 \rightarrow 0.036$
f	78.54	2	4%	1	Circle	$0 \rightarrow 0.036$
g	78.54	2	4%	3	Triangle	$0 \rightarrow 0.036$
h	78.54	2	4%	3	Square	$0 \rightarrow 0.036$
i	78.54	2	4%	3	Pentagon	$0 \rightarrow 0.036$
j	78.54	2	4%	3	Hexagon	$0 \rightarrow 0.036$
k	78.54	2	4%	3	Star	$0 \rightarrow 0.036$

J. Acoust. Soc. Am. **145** (4), April 2019

Zhao et al.   2129
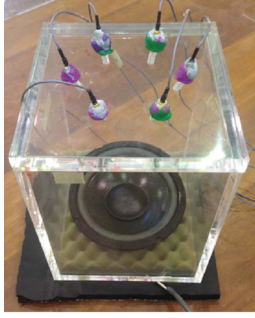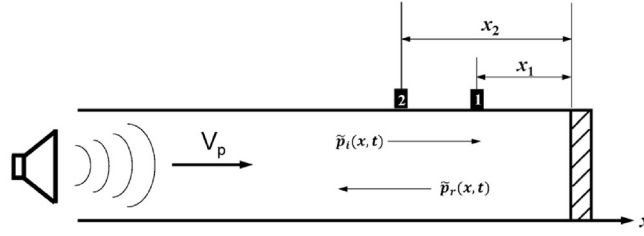
FIG. 4. (Color online) (a) A photo of the designed microphone calibration box used in the anechoic chamber and (b) schematic of a duct with pressure measurements at x_1 and x_2.

microphone are then used to obtain the transfer function (i.e., frequency response). Here microphone 1 is chosen to be a reference. Figure 5 shows the measured amplitude ratio and phase difference between these microphones. It can be seen from Fig. 5 that the amplitude ratios (i.e., gains) are dramatically different. If such a large difference is neglected, then the noise damping performance of the in-duct perforated plates will not be correctly predicted. However, the phase shifts are negligible.

The aeroacoustics damping performances of these perforated plates are quantified and evaluated by determining the power absorption Δ and reflection R coefficients, which have been widely used as a critical index. They are defined as

$$\Delta(\omega) = 1 - \frac{\hat{S}_{CC}(\omega) + \hat{S}_{BB}(\omega)}{\hat{S}_{AA}(\omega) + \hat{S}_{DD}(\omega)}, \quad R(\omega) = \frac{\hat{S}_{BB}(\omega)}{\hat{S}_{AA}(\omega)},$$
(3)

where $\hat{S}_{AA}(\omega)$ and $\hat{S}_{BB}(\omega)$ describe the auto-spectra of decomposed incident and reflected acoustic waves in the upstream of the pipe with an in-duct perforated plate implemented. $\hat{S}_{CC}(\omega)$ and $\hat{S}_{DD}(\omega)$ denote the auto-spectra of the decomposed sound waves in the downstream. These spectra
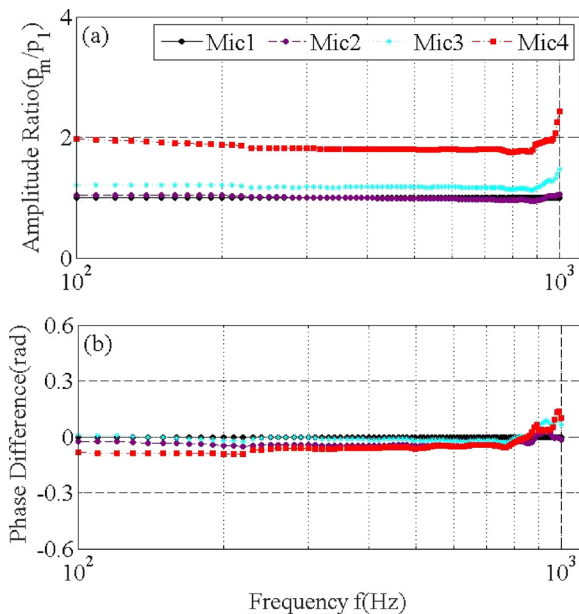

FIG. 5. (Color online) (a) Amplitude ratio and (b) phase difference between the microphone measurements. Microphone 1 is chosen to be the reference.

of the decomposed waves can be estimated by using the conventional two-microphone technique.[30] For completeness, the basic theory of this sound wave decomposition technique is reproduced in the Appendix.

A one-dimensional pipe with plane waves propagating inside and a mean flow with a velocity of ν is considered, as shown in Fig. 4(b). The coordinate origin is assumed to be at the right end of the pipe system. Two pressure sensors/microphones are axially placed at x_1 and x_2. In the current experimental rig, the axial distance, i.e., $|x_2 - x_1|$ between the neighboring two microphones is chosen to be 10 cm. The acoustic waves propagating in the pipe consist of an incident $\tilde{p}_i$ and reflected pressure wave $\tilde{p}_r$ as

$$\tilde{p}_i(x, t) = Ae^{j(\omega t - k_i x)}, \quad \tilde{p}_r(x, t) = Be^{j(\omega t + k_r x)},$$
(4)

where $\omega = 2\pi f$ and f is the forcing frequency. $k_i = \omega/(c_0 + V_p) + (1 - j)\alpha^+$, $k_r = \omega/(c_0 - V_p) + (1 - j)\alpha^-$. c_0 and V_p are the sound speed and the mean flow speed through the duct. $\alpha^{\pm}$ is the damping coefficient.[44] It is determined for typical conditions by visco-thermal dissipation in the thin boundary layer[45] in the duct. More detailed information can be found in Refs. 44 and 45. c_s is the sound speed. The measured pressure perturbation at x_1 or x_2 is given as

$$\tilde{p}_{1,2}(x_{1,2}, t) = \tilde{p}_i(x_{1,2}, t) + \tilde{p}_r(x_{1,2}, t)$$
$$= [Ae^{-jk_i x_{1,2}} + Be^{jk_r x_{1,2}}]e^{j\omega t}.$$
(5)

The power-spectral densities of the pressure measurements at x_1 and x_2 are given as

$$\hat{S}_{mm}(\omega) = \frac{1}{T}\langle \hat{P}_m(\omega), \hat{P}_m^*(f\omega)\rangle,$$
$$\hat{S}_{mn}(\omega) = \frac{1}{T}\langle \hat{P}_m(\omega), \hat{P}_n^*(\omega)\rangle$$
$$= \hat{C}_{mn}(\omega) + j\hat{Q}_{mn}(\omega),$$
(6)

where m denotes 1 or 2. $\hat{P}_m(\omega)$ and $\hat{P}_n(\omega)$ are Fourier transforms of the pressure measurements in time domain at x_m and x_n. And $\hat{P}_m^*(\omega)$ and $\hat{P}_n^*(\omega)$ are complex conjugates of $\hat{P}_m(\omega)$ and $\hat{P}_n(\omega)$. T is the recording period of the pressure data logging. $\hat{S}_{mm}$ is the auto-spectral density of the pressure measurement at x_m. $\hat{S}_{mn}$ is the cross-spectral density between the measured pressure perturbations in time domain at x_m and x_n. $\hat{C}_{mn}(\omega)$ and $\hat{Q}_{mn}(\omega)$ denote the real and imaginary parts of $\hat{S}_{mn}(\omega)$.

These densities are related to the auto-spectral densities of the decomposed incident sound wave $\hat{S}_{AA}(\omega)$, reflected one $\hat{S}_{BB}(\omega)$, and cross-spectral densities $\hat{S}_{AB}(\omega) \equiv \hat{C}_{AB}(\omega) + j\hat{Q}_{AB}(\omega)$, respectively. Here $\hat{C}_{AB}(\omega)$ and $\hat{Q}_{AB}(\omega)$ denote the real and imaginary parts of the cross-spectral density of the decomposed incident and reflected acoustic waves. The relationship can be shown as

$$\left[\hat{S}_{11} \ \hat{S}_{22} \ \hat{C}_{12} \ \hat{Q}_{12}\right]^T = [A]\left[\hat{S}_{AA} \ \hat{S}_{BB} \ \hat{C}_{AB} \ \hat{Q}_{AB}\right]^T, \quad (7)$$

where $[A]$ is a 4×4 coefficient matrix as given in the Appendix. These spectra of $\hat{S}_{AA}(\omega)$, $\hat{S}_{BB}(\omega)$, $\hat{C}_{AB}(\omega)$, and $\hat{Q}_{AB}(\omega)$ are solved by multiplying Eq. (7) with $[A]^{-1}$ as

$$\left[\hat{S}_{AA} \ \hat{S}_{BB} \ \hat{C}_{AB} \ \hat{Q}_{AB}\right]^T = [A]^{-1}\left[\hat{S}_{11} \ \hat{S}_{22} \ \hat{C}_{12} \ \hat{Q}_{12}\right]^T. \quad (8)$$

Note that a similar sound wave decomposition technique can be used to the pressure data logged in the downstream of the pipe with the in-duct perforated plate to calculate the auto- and cross-spectra of $\hat{S}_{CC}(\omega)$, $\hat{S}_{DD}(\omega)$, and $\hat{S}_{CD}(\omega)$. With $\hat{S}_{AA}(\omega)$, $\hat{S}_{BB}(\omega)$, $\hat{S}_{CC}(\omega)$, and $\hat{S}_{DD}(\omega)$ experimentally determined, the sound absorption coefficient Δ and the reflection one R can then be predicted by using Eq. (3).

In order to make our analysis more generalized and to define the limits of the validity of the quasi-steady model as introduced in Sec. IV, a set of dimensionless parameters is introduced. These non-dimensional parameters include the Helmholtz number He, the Strouhal number Sr, and Stokes number S_{to} as defined as

$$\text{He} = \omega D_d / 2\pi c_0,$$
$$\text{Sr} = \omega D_h / (4\pi c_0 M_a) = D_h \text{He}/(2D_d M a),$$
$$\text{St}_o = 1/D_h(8\nu/\omega). \quad (9)$$

Here, M_a is the Mach number through the duct, D_d is the diameter of the duct, and $D_h = 4A_c/P_e$ is the hydraulic diameter of the perforated orifices. P_e is the perimeter of the orifice, and c_0 is the sound speed. The relationship between He and Sr is described in Eq. (9). According to the present experimental flow conditions and the dimensions of the orifices and the duct, the Strouhal and Helmholtz numbers are determined as shown in Figs. 6(a) and 6(b), respectively. It is obvious that He is generally less than 1.0. It implies that the plane wave approximation can be applied to describe the acoustic field at distances greater than the duct diameter from the perforated orifice. The Strouhal number is maximized and approximately $\text{Sr}_{max} = 1.2$ at Mach number $M_a = 0.012$ and the measured maximum frequency $\omega/2\pi = 1000.0 \,\text{Hz}$ and the maximum hydraulic diameter of the orifice $D_h = 10 \,\text{mm}$. However, the Stokes number is negligible $\text{St}_o < 0.01$ and we do not plot it here. Such negligible St_o indicates that viscous dissipation is not dominant.

In Sec. IV, the measured results are illustrated in terms of He, instead of ω. However, if the readers are interested in how the aeroacoustic damping performance Δ/R of the perforated plate depends on acoustic frequency ω, then Fig. 6 and Eq. (9) provides the relationship between He and ω.

IV. RESULTS AND DISCUSSION

Before Δ characterizing the noise damping performance is experimentally determined, the characteristics of the imposed noise generated from the loudspeaker are measured as shown in Fig. 7. The noise frequency is set to 470 Hz and the corresponding Helmholtz number, He, is 0.0603. It can be seen that the measured SPL is approximately 120 dB at $\text{He}_1 = 0.0603$. Furthermore, harmonics are observed at $\text{He}_2 = 0.1206$.
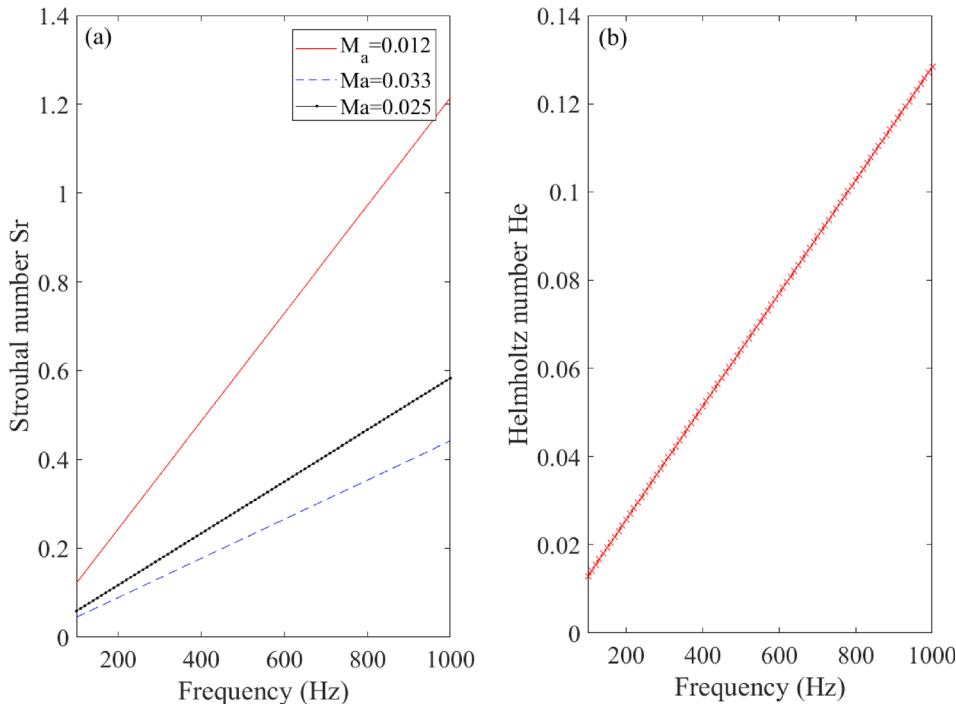

FIG. 6. (Color online) (a) Variation of the Strouhal number and (b) Helmholtz number with the forcing frequency, as the Mach number is set to different values. Note that the Helmholtz number is independent on M_a.

J. Acoust. Soc. Am. **145** (4), April 2019
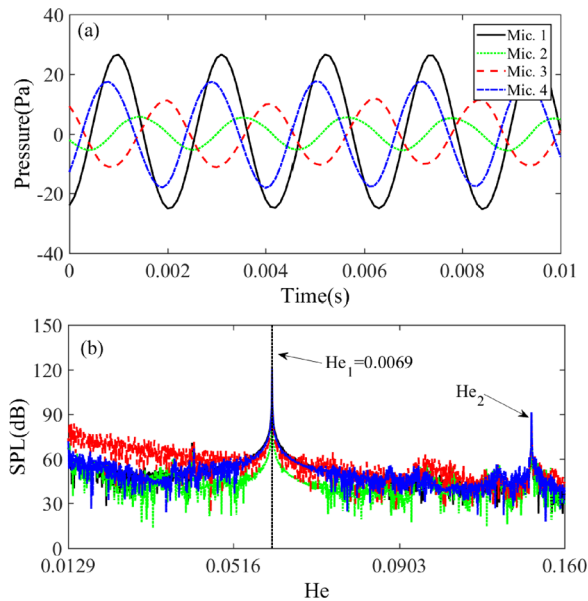
Zhao et al.   2131

FIG. 7. (Color online) (a) time evolution of the measured pressure oscillations from the microphones implemented on both upstream and downstream, and (b) frequency spectra of the measured pressure signals, as $\text{He} = 0.0603$, $M_a = 0.016$ and perforated plate with 1 triangle orifice (see Table I) is implemented.

A. Effect of the orifice geometric shape

In order to evaluate the effect of the orifice geometric shape, perforated plates (a)–(e) are measured in terms of the power absorption coefficient Δ. Figure 8 shows the variation of Δ with Helmholtz number He as $M_a = 0.033$ and $N = 1$. It can be seen that there are 5 local Δ_{max} from $\text{He} = 0.0129$ to 0.129 (corresponding to $100 \leq \omega/2\pi \leq 1000\,\text{Hz}$). The corresponding Helmholtz numbers He_m for $m = 1$ to 5 are denoted by He_1 to He_5. The multiple power absorption peaks are due to the periodic reflection coefficient of the cold-flow open-ended pipe. When the Helmholtz number $\text{He} \leq (\text{He}_3 + \text{He}_4)/2$,

power absorption coefficient Δ depends little on the geometric shape of the perforated orifices. However, as He is further increased to He_5, the perforated plate with pentagon-shaped (Pe) orifice is associated with the largest local Δ_{max}. The star-shaped (St) orifice is found to be the smallest local Δ_{max}. This is most likely due to the longest wetted perimeter and much decreased acoustic impedance. This reveals that the orifice geometric shape strongly affects the damping performance of a higher Helmholtz number noise (see the shaded area of Fig. 8.). This is most likely due to the shorter wavelength, which is comparable with the orifice dimensions. At low Helmholtz number, the noise wavelength is larger than the characteristic length of the different shaped orifices. Thus, the orifice shape does not alter its damping performance at a lower He.

In certain applications, there are other definitions which are more appropriate for determining the performance of a noise damping device. An acoustic damper is often applied to prevent acoustic disturbances in a duct from returning to its source. In this way, the growth of acoustically-driven flow/thermoacoustic instabilities might be mitigated. One of the widely alternative definitions is reflection coefficient R as defined in Eq. (3). The measured reflection coefficient R varied with the Helmholtz number He is shown in Fig. 9.

The flow conditions and implemented orifices are set to be the same as those in Fig. 8. It can be seen from Fig. 9 that there are five local minimum reflection coefficients R_{min}, which are corresponding to the local Δ_{max} as shown in Fig. 8. The St orifice is associated with the smallest local R_{min} at $\text{He} < 0.1161$. However, as He is increased, the Tr orifice has the smallest local R_{min}. However, the St orifice is changed to be with the largest local R_{max}, while it has local minimum Δ_{max} (see Fig. 8). When local R_{max} is concerned, there is little difference between different shaped orifices at $\text{He} \leq 0.1161$ (corresponding to $\omega/2\pi \leq 900\,\text{Hz}$). However, as He is increased, the orifice shape does affect local R_{max} (see the shaded area of Fig. 9).
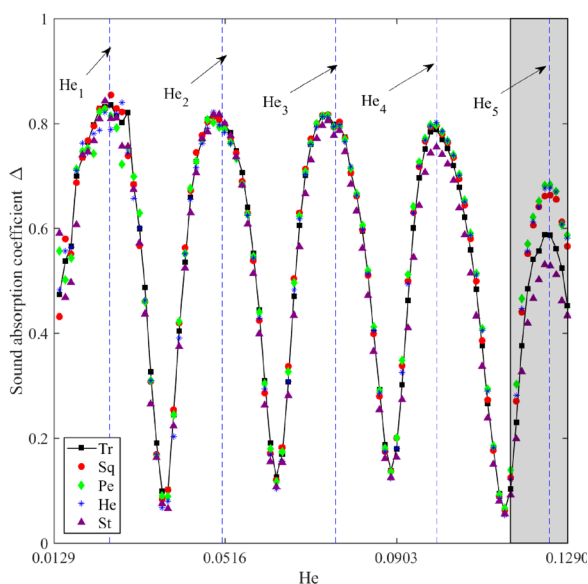

FIG. 8. (Color online) Comparison of the power absorption coefficient Δ measured from perforated plates (a) Tr, (b) Sq, (c) Pe, (d) Hx, and (e) St, as $M_a = 0.033$ and $N = 1$.
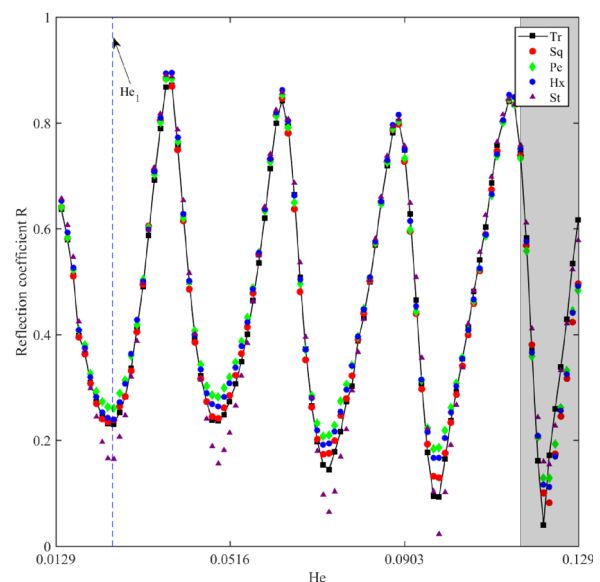

FIG. 9. (Color online) Comparison of the measured reflection coefficient from perforated plates (a)–(e), as $M_a = 0.033$ and $N = 1$.

To validate our findings, perforated plates (g)–(k) (see Table I) are experimentally tested. The main difference between these plates and the previous used ones are the number of perforated orifices. These plates (g)–(k) are associated with three orifices perforated on each plate. The measurements are summarized in Fig. 10.

It can be seen from Fig. 10(a) that the Pe orifices are associated with the largest local maximum power absorption Δ_{max}. And the St orifices are with the smallest local Δ_{max}. The orifice shape effect is clearly observed as $He > 0.0903$, which is smaller than that observed in the perforated plates with only 1 orifice, i.e., $N = 1$. When the reflection coefficient R is considered, as shown in Fig. 10(b), the St orifices are associated with the smallest local R_{min}. It is worth noting that there are other shaped perforations, such as slits with the Stokes number in the order of unity. Such slit perforations have a width on the order of 0.05 mm. Different noise damping behaviors as discussed in the previous works[39,49] are expected. Interested readers can refer to Refs. 39 and 49. However, the present work focuses on the current six shaped orifices. Further studies are needed to study more different shaped perforations.

B. Effect of the Mach number M_a

Now let us examine the effect of mean flow Mach number M_a on the noise absorbing performance of the perforated plates with different geometric shaped orifices. Figure 11 illustrates the noise damping performance of the in-duct perforated plate (a), i.e., Tr orifice, as $N = 1$ and the bias flow Mach number is set to 5 different values. It can be seen that the local maximum power absorption Δ and reflection coefficients R are periodically present across the Helmholtz number from 0.0129 to 0.129 at He_m. As there is no mean flow,
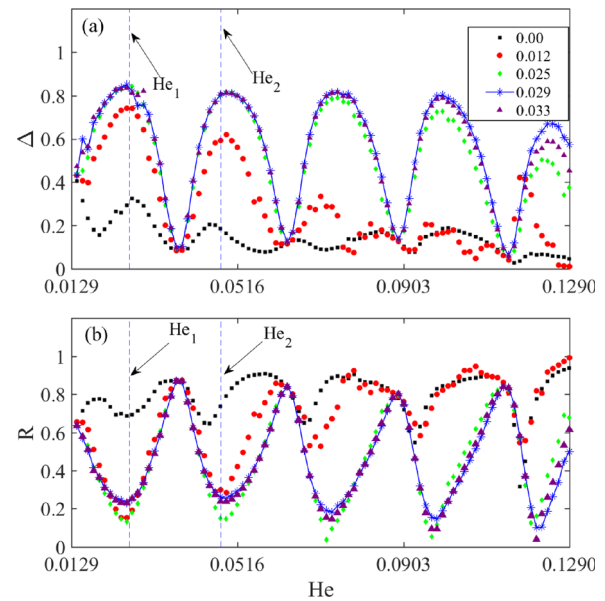
FIG. 11. (Color online) Comparison of the power absorption Δ and reflection coefficient R measured from the perforated plate (a) with Tr orifice, as $N = 1$ and the bias flow Mach number M_a is set to 5 different values.

i.e., $M_a = 0$, the power absorption coefficient Δ is very small and the reflection coefficient is very large. The periodic change in Δ and R are not so obvious. However, as M_a is increased, the power absorption and reflection coefficients are increased dramatically. Maximum power absorption is approximately 0.83. Further increasing M_a leads to the local Δ_{max} being decreased at high He (see the local peak at $0.114 \leq He \leq 0.129$). Maximum power absorption coefficient Δ_{max} is obtained, as $M_a = 0.029$. This graph confirms that the mean flow plays an important role on affecting the damping performance of the perforated orifice. And there is an optimum Mach number corresponding to the maximum noise damping performance.

Figure 11 also reveals the transition from quasi-steady flow behaviors to essentially unsteady behaviors. To shed light on the transition, the measured aeroacoustic damping coefficients Δ and R are discussed in terms of the Strouhal number. When $M_a = 0.012$ and $He < 0.0516$ (corresponding to $Sr < 0.49$), Δ and R are related strongly to the Strouhal number. As M_a is increased to 0.025, the sound absorption and reflection coefficients depend significantly on the Strouhal number, i.e., $Sr < 0.46$. Similar dependency trends are observed as M_a is set to 0.029 and 0.033.

The mean flow effect on Δ_{max} and R_{min} is observed, as the perforated plate (e) with St orifices is implemented. The experimental results are summarized in Fig. 12. It can be seen that as M_a is increased, the local Δ_{max} is increased first and local R_{min} is decreased first. Maximum power absorption occurs as $M_a = 0.033$. However, minimum reflection R_{min} occurs at $M_a = 0.025$. This indicates that the optimum mean flow velocity corresponding to Δ_{max} depends on the orifice shape.

C. Effect of the number N of orifices

There is an interest of knowing the effect of the number N of the same-shaped orifices on its damping performance,
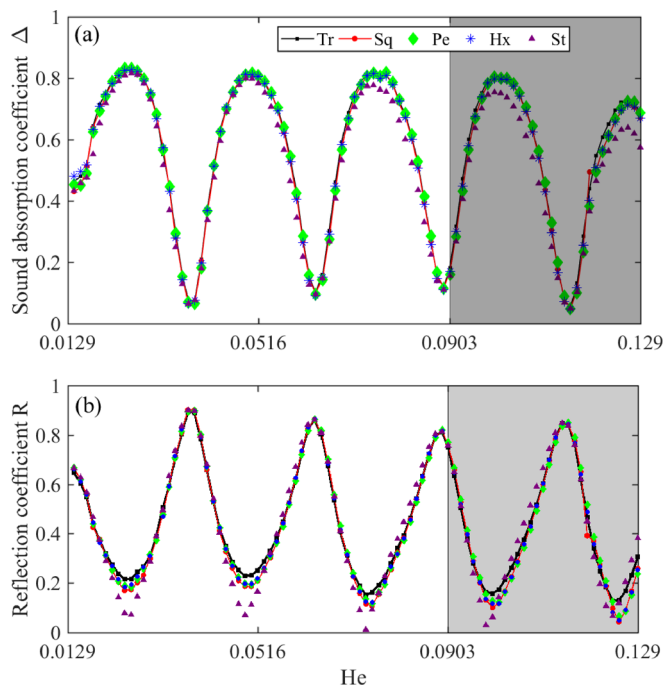

FIG. 10. (Color online) Comparison of the measured reflection coefficient from the perforated plates (f)–(j), as $M_a = 0.033$ and $N = 3$.
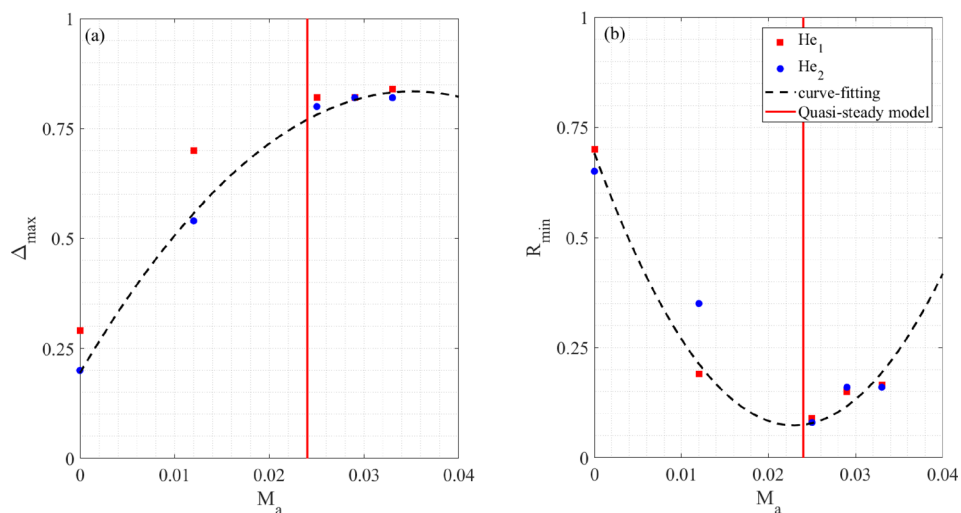
FIG. 12. (Color online) Variation of the measured local maximum power absorption Δ_{max} and local minimum reflection coefficient R_{min} with M_a from the perforated plate with a St orifice, as $N = 1$ and He is set to He_1 and He_2, respectively.

when the porosity remains the same. Figure 13 shows the comparison of the power absorption coefficients measured from the in-duct perforated plates (a)–(e), as $M_a = 0.033$ and N is set to 2 values. It can be observed that at low Helmholtz number (He < 0.1161), the damping performance is almost the same, as N is varied. This observation is applicable to all shaped orifices [see Figs. 13(b)–13(e)]. The maximum power absorption Δ_{max} is approximately 0.85,

independent on the orifice shape. However, as the Helmholtz number He is increased, the perforated plated with more orifices absorbed more noise than that with less number of perforated orifices, as shown in the shaded area of Figs. 13(a)–13(e). Closer observation of the Tr and St orifices [see Figs. 13(a) and 13(e)] reveals that 20% more sound is absorbed at He ≈ 0.1244 as denoted by the green dashed-dotted line. This is most likely due to the fact that the sound
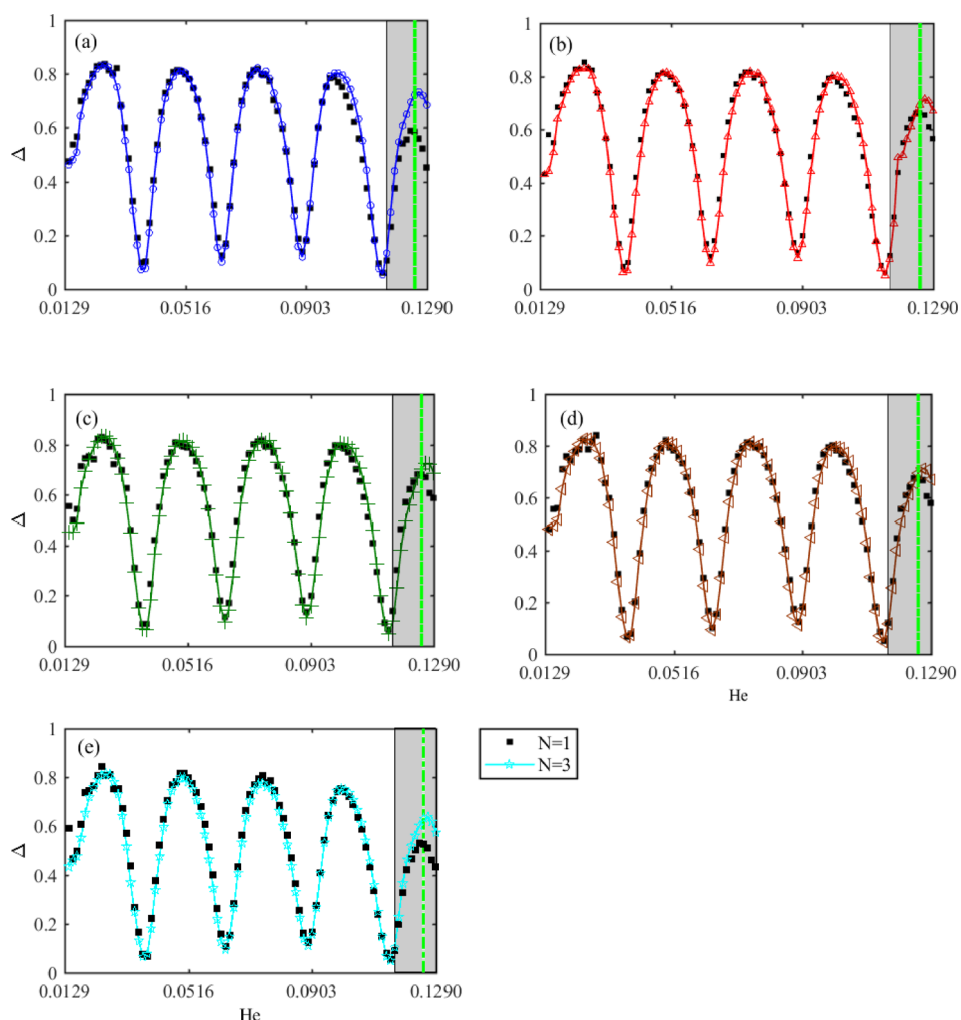

FIG. 13. (Color online) Comparison of the power absorption coefficient Δ measured from the in-duct perforated plate with (a) triangle-, (b) square-, (c) pentagon-, (d) hexagon-, and (e) star-shaped orifice, as $M_a = 0.033$ and N is set to two different values.

wavelength at a higher Helmholtz number is comparable with the characteristic length of the orifice.

From an engineering point of view, acoustic liners with circle-shaped perforated orifices are widely applied.[32–34] The damping performances of these perforated plates as tested above is compared to that of a perforated plate with a circle-shaped orifice as shown in Fig. 14. Note that the plate's porosity remains as 4%.

It can be seen that all the Δ measurements over the Helmholtz number range are almost the same. However, a closer observation reveals that the circle shaped orifice is associated with a slightly larger Δ, as $\text{He} > 0.1032$. However, it has a smaller Δ over certain Helmholtz number ranges, for example $0.0872 \leq \text{He} \leq 0.0975$ and $0.0616 \leq \text{He} \leq 0.0706$. The variation of Δ of the circle-shaped orifice in comparison of that of other shaped ones makes it difficult to determine an optimum design. The wide application of circle-shaped perforated orifices[35,36] may be the fact that they are to easier and low-cost to fabricate.

In general, it is shown that perforated plates[37,38] with the same porosities can dissipate noise effectively, depending on (1) the geometric shape and (2) the number of the orifices, (3) Mach number M_a (Ref. 39) and (4) the Helmholtz number range.[40,41] At a certain frequency, the incident sound waves in the duct with a mean flow[42,43] might be 100% reflected back. And approximately 85% of the incident sound can be absorbed.

V. QUASI-STEADY ANALYSIS OF AEROACOUSTICS DAMPING OF PERFORATED ORIFICES

For a low Strouhal number (i.e., $S_r < 0.45$) and $M_a \ll 1.0$, a quasi-steady incompressible flow[44,46] is assumed to pass the perforated orifices. If pressure recovery in the downstream jet

FIG. 14. (Color online) Comparison of the power absorption coefficient Δ measured from the in-duct perforated plate with (a) triangle-, (b) square-, (c) pentagon-, (d) hexagon-, (e) star-, and (f) circle-shaped orifice, as $M_a = 0.033$ and $N = 1$.

is neglected, then the mass conservation and Bernoulli equations hold as

$$\rho_0 A_j \tilde{v}_j = A_p (\rho_0 \tilde{v}_p + \tilde{\rho}_p V_p), \tag{10}$$

$$\tilde{v}_j V_j = (\tilde{p}_p / \rho_0 + \tilde{v}_p V_p). \tag{11}$$

Here subscripts j and p denote the jet through the orifice and the pipe. V_j and $V_p = c_0 M_a$ are the mean flow speeds of the orifice jet and through the duct, respectively. c_0 is the sound speed. The tilde denotes the flow fluctuation. Note that the mean flow mass conservation also holds as $\rho_0 A_j V_j = \rho_0 A_p V_p$. The cross-sectional area A_j of the jet is related to the orifice cross-sectional area as $A_j = A_o V_c$. Here V_c is the vena contracta factor $V_c = \pi/(\pi + 2) \approx 0.6$.[46,48] The vena contracta effect is neglected in the previous work by Ingard and Labate.[9] There is also an error in Moers et al.[39] The formula for the acoustic velocity through the orifice misses a geometric dimension factor h_w/A_p of the wall perforation. A correct definition is given by Tonon et al.[49]

Applying the traveling plane wave model $\tilde{p}_p = \tilde{p}_i + \tilde{p}_r$, $\tilde{v}_p = (\tilde{p}_i - \tilde{p}_r)/\rho_0 c_0$, $\tilde{\rho}_p = (\tilde{p}_i + \tilde{p}_r)/c_0^2$ and conducting further simplification leads to the reflection coefficient being determined as

$$R(\omega) = \left| \frac{\tilde{p}_r e^{-j\omega t}}{\tilde{p}_i e^{-j\omega t}} \right| = \left| -\frac{\left(1 + \dfrac{A_j M_a}{A_p}\right)\left(1 - \dfrac{A_p M_a}{A_j}\right)}{\left(1 + \dfrac{A_p M_a}{A_j}\right)\left(1 - \dfrac{A_j M_a}{A_p}\right)} \right|. \tag{12}$$

It can be seen from Eq. (12) that when acoustic radiation at the duct termination and visco-thermal losses are neglected,[47] the reflection coefficient R will vanish at $M_a = A_j/A_p$. When the vena contracta factor V_c,[46,48] the minimum reflection coefficient $R_{\min}$ is obtained as $M_a \approx 0.024$. This agrees well with the experimental measurements as shown in Fig. 12(b). A similar quasi-steady model of perforated liners with bias flow was recently discussed in Refs. 50 and 51.

Not that a similar but less pronounced deviation of the triangle shaped orifices for $N = 1$, $M_a = 0.033$, and $\text{He} > 0.1161$ is shown in Fig. 14. However, there are some differences in power absorption behaviors between the star and other geometries. This may be due to the fact that (1) the orifices edges are not perfectly sharp and this induces an increase of vena contracta ratio around the edges of the star shaped orifices, and (2) the effect of the Stokes layers at the edges of the star.

VI. CONCLUSIONS

In this work, 11 perforated plates are designed and experimentally tested in a cold-flow duct with a controllable low Mach number flow. These plates have the same porosity of 4% but different geometric shapes of orifices: (1) triangle, (2) square, (3) pentagon, (4) hexagon, (5) star, and (6) circle. The effects of (1) the mean flow, (2) the geometric shape, and (3) the number of perforated orifices are examined one at a time to gain insights on the noise absorbing performance of these in-duct perforated plates. The damping effect is
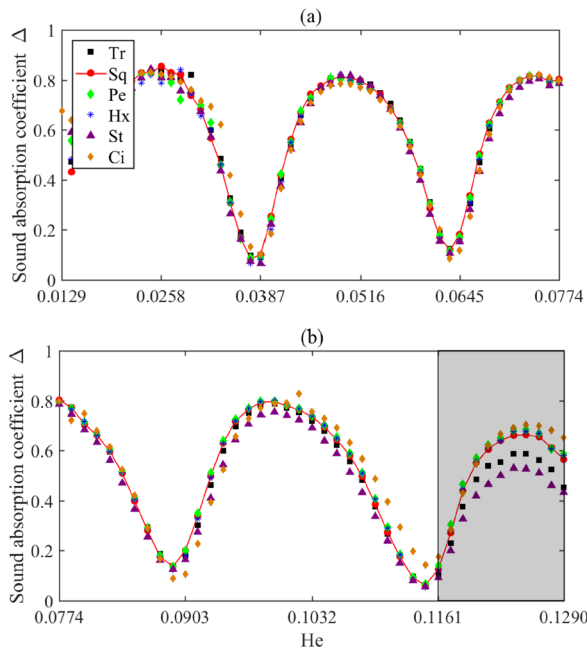
J. Acoust. Soc. Am. **145** (4), April 2019

Zhao et al. 2135

characterized by using power absorption coefficient Δ and reflection coefficient R, which are measured with the dimensionless Helmholtz number varied from 0.0129 to 0.129. The noise damping performance is found to be either improved or deteriorated, depending on (1) the Helmholtz number He, (2) the bias flow Mach number M_a, (3) geometric shape of the orifices, and (4) the number N of the orifices. It is interesting to find that the six different shapes of the perforated orifices are associated with almost the same local maximum power absorption coefficient Δ_{max} at He ≈ 0.0244, 0.0487, and 0.0731. However, as the Helmholtz number is increased (He ≥ 0.0903), St-shaped orifices are found to be associated with the lowest Δ. But circle (Ci) and Pe-shaped orifices are with a larger Δ. For the perforated plates with the same shaped orifice and same porosity, increasing the number N of perforated orifices is shown to lead to an increase of Δ. Tr- and St-shaped orifices are found to be associated with 20% more sound being absorbed at approximately He = 0.1244. However, at lower He (≤ 0.1161), the power absorption is found to be little changed. This is most likely due to the comparable wavelength with the characteristic length of the orifices. Approximately 85% of incident plane waves is absorbed, i.e., $\Delta_{max} \approx 0.85$, as $M_a \geq 0.029$. The optimum bias flow Mach number corresponding to Δ_{max} is shown to depend on the orifice shape. To shed light on the orifice damping behaviors, the quasi-steady model could be applied, depending on the Strouhal number. According to the present measurements, the transition from quasi-steady flow behaviors to unsteady behaviors occurs at approximately Sr = 0.45. The predicted optimum Mach number from the quasi-steady model corresponding to the minimum reflection coefficient R_{min} agrees well with the experimental measurements. In general, the present parametric measurements reveals the critical roles of (1) the mean flow, (2) geometric shape, and (3) the number of perforated orifices on its noise damping capacity, especially at higher He ≥ 0.0903. The findings facilitate the design of effective perforated liners.

It is worth noting the present findings are obtained over the frequency range of 100 to 1000 Hz. These concluding remarks may not be applicable to higher frequency (for example, 2000 to 5000 Hz) acoustic disturbances, since the corresponding wavelength is much smaller. The orifices' shape effect may be more dominant. However, this needs further experimental testes to confirm it.

ACKNOWLEDGMENTS

APPENDIX: COEFFICIENT MATRIX [A]

The elements of the coefficient matrix [A] involved in the classical two-microphone technique[30] is given as

$$[\mathbf{A}]_{11} = 1, \quad [\mathbf{A}]_{12} = 1, \quad [\mathbf{A}]_{13} = 2\cos(k_i + k_r)x_1,$$
$$[\mathbf{A}]_{14} = 2\sin(k_i + k_r)x_1,$$

$$[\mathbf{A}]_{21} = 1, \quad [\mathbf{A}]_{22} = 1, \quad [\mathbf{A}]_{23} = 2\cos(k_i x_2 + k_r x_2),$$
$$[\mathbf{A}]_{24} = 2\sin(k_i x_2 + k_r x_2),$$

$$[\mathbf{A}]_{31} = \cos(k_i x_1 - k_i x_2), \quad [\mathbf{A}]_{32} = \cos(k_r x_1 - k_r x_2),$$

$$[\mathbf{A}]_{33} = \cos(k_i x_2 + k_r x_1) + \cos(k_r x_2 + k_i x_1),$$

$$[\mathbf{A}]_{34} = \sin(k_i x_2 + k_r x_1) + \sin(k_r x_2 + k_i x_1),$$

$$[\mathbf{A}]_{41} = \sin(k_i x_1 - k_i x_2), \quad [\mathbf{A}]_{42} = -\sin(k_r x_1 - k_r x_2),$$

$$[\mathbf{A}]_{43} = \sin(k_r x_1 + k_i x_2) - \sin(k_r x_2 + k_i x_1),$$

$$[\mathbf{A}]_{44} = \cos(k_i x_2 + k_r x_1) - \cos(k_r x_2 + k_i x_1).$$

Note that a new two-microphone technique is proposed by Melling *et al.*[40] and experimentally tested for broadband noise.[52,53] Interested readers can refer to the previous work.[40]

[1]G. A. Richards, D. L. Straub, and E. H. Robey, "Passive control of combustion dynamics in stationary gas turbines," J. Propul. Power **19**, 795–810 (2003).

[2]G. Wu and Z. Lu, "Numerical and experimental demonstration of actively passive mitigating self-sustained thermoacoustic oscillations," Appl. Energy **222**, 257–266 (2018).

[3]C. Lahiri and F. Bake, "A review of bias flow liners for acoustic damping in gas turbine combustors," J. Sound Vib. **400**, 564–605 (2017).

[4]D. J. Bodony and S. K. Lele, "On using large-eddy simulation for the prediction of noise from cold and heated turbulent jets," Phys. Fluids. **17**, 085103 (2005).

[5]C. Z. Ji and D. Zhao, "Lattice Boltzmann investigation of acoustic damping mechanism and performance of an in-duct circular orifice," J. Acoust. Soc. Am. **135**(6), 3243–3251 (2014).

[6]J. C. Wendoloski, "Sound absorption by an orifice plate in a flow duct," J. Acoust. Soc. Am. **104**(1), 122–132 (1998).

[7]X. Sun, X. Jing, H. Zhang, and Y. Shi, "Effect of grazing-bias flow interaction on acoustic impedance of perforated plates," J. Sound Vib. **254**(3), 557–573 (2002).

[8]X. Jing and X. Sun, "Experimental investigations of perforated liners with bias flow," J. Acoust. Soc. Am. **106**, 2436–2441 (1999).

[9]U. Ingard and S. Ingard, "Acoustic circulation effects and the nonlinear impedance of orifices," J. Acoust. Soc. Am. **22**, 211–218 (1950).

[10]I. Hughes and A. P. Dowling, "The absorption of sound by perforated linings," J. Fluid Mech. **218**, 299–335 (2006).

[11]J. D. Eldredge and A. P. Dowling, "The absorption of axial acoustic waves by a perforated liner with bias flow," J. Fluid Mech. **485**, 307–335 (2003).

[12]S. M. Grace, K. P. Horan, and M. S. Howe, "The influence of shape on the Rayleigh conductivity of a wall aperture in the presence of grazing flow," J. Fluid Struct. **12**(3), 335–351 (1998).

[13]M. Howe, "On the theory of unsteady high Reynolds number flow through a circular aperture," Proc. Royal Soc. London Series A **366**(1725), 205–223 (1979).

[14]A. Kierkegaard, S. Boij, and G. Efraimsson, "A frequency domain linearized Navier-Stokes equations approach to acoustic propagation in flow ducts with sharp edges," J. Acoust. Soc. Am. **127**(2), 710–719 (2010).

[15]D. Zhao, A. S. Morgans, and A. P. Dowling, "Tuned passive control of acoustic damping of perforated liners," AIAA J. **49**(4), 725–734 (2011).

[16]Z. Zhong and D. Zhao, "Time-domain characterization of the acoustic damping of a perforated liner with bias flow," J. Acoust. Soc. Am. **132**(1), 271–281 (2012).

[17]C. K. W. Tam, K. A. Kurbatskii, K. K. Ahuja, and R. J. Gaeta, "A numerical and experimental investigation of the dissipation mechanisms of resonant acoustic liners," J. Sound Vib. **245**(3), 545–557 (2001).

[18]S. Mendez and J. D. Eldredge, "Acoustic modeling of perforated plates with bias flow for large-eddy simulations," J. Comput. Phys. **228**(13), 4757–4772 (2009).

[19]Q. Zhang and D. J. Bodony, "Numerical investigation and modelling of acoustically excited flow through a circular orifice backed by a hexagonal cavity," J. Fluid Mech. **693**, 367–401 (2012).

[20]J. Su, J. Rupp, A. Garmory, and J. F. Carrotte, "Measurements and computational fluid dynamics predictions of the acoustic impedance of orifices," J. Sound Vib. **352**, 174–191 (2015).

[21]A. R. da Silva, G. P. Scavone, and A. Lefebvre, "Sound reflection at the open end of axisymmetric ducts issuing a subsonic mean flow: A numerical study," J. Sound Vib. **327**(3–5), 507–528 (2009).

[22]C. Ji and D. Zhao, "Two-dimensional lattice Boltzmann investigation of sound absorption of perforated orifices with different geometric shapes," Aerosp. Sci. Tech. **39**, 40–47 (2014).

[23]P. T. Lew, L. Mongeau, and A. Lyrintzis, "Noise prediction of a subsonic turbulent round jet using the lattice-Boltzmann method," J. Acoust. Soc. Am. **128**(3), 1118–1127 (2010).

[24]E. Vergault and P. Sagaut, "An adjoint-based Lattice Boltzmann method for noise control problems," J. Comput. Phys. **276**(1) 39–61 (2014).

[25]E. W. S. Kam, R. M. C. So, and R. C. K. Leung, "Lattice Boltzmann method simulation of aeroacoustics and nonreflecting boundary conditions," AIAA J. **45**(7), 1703–1712 (2007).

[26]V. Bellucci, P. Flohr, and C. O. Paschereit, "Numerical and experimental study of acoustic damping generated by perforated screens," AIAA J. **42**(8), 1543–1549 (2004).

[27]X. Jing and X. Sun, "Sound-excited flow and acoustic nonlinearity at an orifice," Phys. Fluids **14**(1), 268–276 (2002).

[28]R. Leung, R. So, M. Wang, and X. Li, "In-duct orifice and its effect on sound absorption," J. Sound Vib. **299**(4–5), 990–1004 (2006).

[29]X. Jing and X. Sun, "Effect of plate thickness on impedance of perforated plates with bias flow," AIAA J. **38**(9), 1573–1578 (2000).

[30]A. F. Seybert and D. F. Ross, "Experimental determination of acoustic properties using a two-microphone random-excitation technique," J. Acoust. Soc. Am. **61**(5), 1362–1370 (1977).

[31]D. Zhao, "A real-time plane-wave decomposition algorithm for characterizing perforated liners damping at multiple mode frequencies," J. Acoust. Soc. Am. **129**(3), 1184–1192 (2011).

[32]R. J. Gaeta and K. K. Ahuja, "Effect of orifice shape on acoustic impedance," Int. J. Aeroacoust. **15**(4–5), 474–495 (2016).

[33]C. Lawn, "The acoustic impedance of perforated plates under various flow conditions relating to combustion chamber liners," Appl. Acoust. **106**, 144–154 (2016).

[34]D. Haufe, A. Schulz, F. Bake, L. Enghardt, J. Czarske, and A. Fischer, "Spectral analysis of the flow sound interaction at a bias flow liner," Appl. Acoust. **81**, 47–49 (2014).

[35]V. Phong and D. Papamoschou, "Acoustic transmission loss of perforated plates," J. Acoust. Soc. Am. **134**(2), 1090–1101 (2013).

[36]E. Gullaud and F. Nicoud, "Effect of perforated plates on the acoustics of annular combustors," AIAA J. **50**(12), 2629–2642 (2012).

[37]S. H. Lee, J. G. Ih, and K. S. Peat, "A model of acoustic impedance of perforated plates with bias flow considering the interaction effect," J. Sound Vib. **303**(3–5), 741–752 (2007).

[38]R. J. Astley, R. Sugimoto, and P. Mustafi, "Computational aeroacoustics for fan duct propagation and radiation, current status and application to turbofan liner optimization," J. Sound Vib. **330**(16), 3832–3845 (2011).

[39]E. Moers, D. Tonon, and A. Hirschberg, "Strouhal number dependency of the aeroacoustic response of wall perforations under combined grazing-bias flow," J. Sound Vib. **389**, 292–308 (2017).

[40]J. Melling, J. Chen, and P. Joseph, "Experimental investigation of a new two-microphone method for the determination of broadband noise radiation from ducts," Appl. Acoust. **117**, 66–75 (2017).

[41]N. Noiray, D. Durox, T. Schuller, and S. Candel, "Passive control of combustion instabilities involving premixed flame anchored on perforated plate," Proc. Combust. Inst. **31**(1), 1283–1290 (2007).

[42]I. Dupere and A. Dowling, "The absorption of sound near abrupt axisymmetric area expansions," J. Sound Vib. **239**(4), 709–730 (2001).

[43]D. Yang and A. S. Morgans, "A semi-analytical model for the acoustic impedance of finite length circular holes with mean flow," J. Sound Vib. **384**, 294–311 (2016).

[44]P. Durrieu, G. Hofmans, G. Ajello, R. Boot, Y. Auregan, A. Hirschberg, and M. Peters, "Quasi-steady aeroacoustic response of orifices," J. Acoust. Soc. Am. **110**(4), 1859–1872 (2001).

[45]D. Ronneberger and C. Ahrens, "Wall shear stress caused by small amplitude perturbations of turbulent boundary layer flow: An experimental investigation," J. Fluid Mech. **83**(3), 433–464 (1977).

[46]G. C. J. Hofmans, M. Ranucci, G. Ajello, Y. Auregan, and A. Hirschberg, "Aeroacoustic response of a slit-shaped diaphragm in a pipe at low Helmholtz number: 1 quasi-steady results," J. Sound Vib. **244**(1), 57–77 (2001).

[47]D. W. Bechert, "Sound absorption caused by vorticity shedding demonstrated with a jet flow," J. Sound Vib. **70**(3), 389–405 (1980).

[48]A. Cummings and W. Eversman, "High amplitude acoustic transmission through duct terminations: Theory," J. Sound Vib. **91**(4), 503–518 (1983).

[49]D. Tonon, E. M. T. Moers, and A. Hirschberg, "Quasi-steady acoustic response of wall perforations subject to a grazing-bias flow combination," J. Sound Vib. **332**(7), 1654–1673 (2013).

[50]G. Regunath, J. Rupp, and J. F. Carrotte, "Acoustic quasi-steady response of thin walled perforated liners with bias and grazing flows," J. Sound Vib. **412**, 424–440 (2018).

[51]A. Scarpato, N. Tran, S. Ducruix, and T. Schuller, "Modeling the damping properties of perforated screens traversed by a bias flow and backed by a cavity at low Strouhal number," J. Sound Vib. **331**(2), 276–290 (2012).

[52]Y. Meng, L. Wu, X. Jing, and X. Sun, "Acoustic behavior of an aperture backed by sound absorbing materials under grazing flow," J. Sound Vib. **446**, 73–90 (2019).

[53]X. Dai, X. Jing, and X. Sun, "Acoustic-excited vortex shedding and acoustic nonlinearity at a rectangular slit with bias flow," J. Sound Vib. **333**(13), 2713–2727 (2014).

J. Acoust. Soc. Am. **145** (4), April 2019

Zhao *et al.*   2137